

Nonclassical correlations in damped quantum solitons

Eduard Schmidt, Ludwig Knöll, and Dirk-Gunnar Welsch
*Friedrich-Schiller-Universität Jena, Theoretisch-Physikalisches Institut
 Max-Wien Platz 1, D-07743 Jena, Germany*
 (February 5, 2020)

Using cumulant expansion in Gaussian approximation, the internal quantum statistics of damped soliton-like pulses in Kerr media are studied numerically, considering both narrow and finite bandwidth spectral pulse components. It is shown that the sub-Poissonian statistics can be enhanced, under certain circumstances, by absorption, which damps out some destructive interferences. Further, it is shown that both the photon-number correlation and the correlation of the photon-number variance between different pulse components can be highly nonclassical even for an absorbing fiber. Optimum frequency windows are determined in order to realize strong nonclassical behavior, which offers novel possibilities of using solitons in optical fibers as a source of nonclassically correlated light beams.

I. INTRODUCTION

Nonclassical features of optical pulses like squeezing, sub-Poissonian statistics and entanglement have been of increasing interest for optical communication and measurement techniques [1–4]. From classical optics it is well known that in fibers photons can fly in soliton-like pulses over long distances, provided that they intense enough and the fiber nonlinearity can compensate for the dispersion-assisted pulse spreading [5,6]. Yet solitons are not rigid but very lively nonclassical species, because of the quantum noise associated with the nonlinear dynamics. Since already single-mode radiation becomes nonclassical under the influence of a Kerr nonlinearity [7], solitons can be expected to exhibit not only single-mode nonclassical properties but also nonclassical internal correlations.

The study of quantum solitons has been also motivated by a number of possible applications [1,2,4]. Solitons may be used for realizing efficient and reliable sources of pulses with intensity fluctuations below the shot noise level. Nondestructive high-precision optical switching devices and logic gates may be implemented applying the concept of quantum non-demolition measurement to the collision interaction of solitons [8–10]. Suppression of noise in soliton communication lines [1,2,4] and usage of solitons in quantum information processing [4] may be other potential applications.

Nonclassical properties of optical solitons have been detected in a number of experiments. In [11,12] soliton squeezing is measured using homodyne detection. Photon-number squeezing of the spectrally filtered solitons is measured by direct detection in [13,14]. In the experiment in [15] with asymmetrical (10/90) fiber-loop interferometer photon-number squeezing up to 6.0dB is achieved. Recently the experimental studies have been extended to internal spectral photon-number correlations associated with narrow bandwidth soliton components [16].

Disregarding losses, the dynamics of quantum solitons in optical fibers may be described by the operator-valued nonlinear Schrödinger equation, which can be solved employing the Bethe ansatz [17]. The method was used successfully to calculate field and intensity correlations in the space-time domain [18,19]. In practice however, the quantum nonlinear Schrödinger equation must be modified by supplementing it with further terms in order to include effects such as absorption, third-order dispersion, and Raman scattering. Various methods of solution have been developed and successfully applied [20–34].

Here we follow [34] and use cumulant expansion in Gaussian approximation for studying spectral photon-number squeezing and nonclassical photon-number correlation of different spectral components of damped solitons. We consider both narrow-bandwidth spectral pulse components [16] and pulse components with finite spectral bandwidth selected by optimally chosen square bandpass filters [30]. The numerically obtained results illustrate the possibility to use optical solitons for generation of squeezed light and nonclassically correlated light beams also in the presence of absorption. Moreover, the results reveal that absorption can improve, under certain circumstances, the nonclassical features.

The article is organized as follows. Section II outlines the used basic concept. The relations necessary for studying nonclassical correlations are given in Sec. III, and the numerical results are reported in Sec. IV. Finally, a summary and some concluding remarks are given in Sec. V.

II. BASIC CONCEPT

Let us first give a brief outline of the used concept for describing the propagation of a quantized optical pulse through an absorbing fiber with second order dispersion and Kerr nonlinearity (for details, see [34] and references therein). The spatio-temporal pulse evolution in a co-moving reference frame is described in terms of slowly

varying bosonic operators $\hat{a}(x, t)$ satisfying the commutation relation

$$[\hat{a}(x, t), \hat{a}^\dagger(x', t')] = \mathcal{A}^{-1} \delta(x - x'), \quad (1)$$

[\mathcal{A} is the effective cross-section of the fiber]. The undamped motion is governed by the Hamiltonian

$$\hat{H} = \hbar \mathcal{A} \int dx \left[\frac{1}{2} \omega^{(2)} (\partial_x \hat{a}^\dagger) (\partial_x \hat{a}) + \frac{1}{2} \chi \hat{a}^\dagger \hat{a}^\dagger \hat{a} \hat{a} \right], \quad (2)$$

where the constant χ is related to the third-order susceptibility $\chi^{(3)}$ as

$$\chi = \frac{3\chi^{(3)}\hbar(v_{\text{gr}}k_c)^2}{4\epsilon_r^2\epsilon_0} \quad (3)$$

[ϵ_r , relative permittivity at the carrier frequency ω_c ; k_c , carrier wave number; v_{gr} , group velocity; $\omega^{(2)} = d^2\omega(k)/dk^2|_{k=k_c}$]. Note that solitons can be formed either in focusing media with anomalous dispersion ($\chi < 0$, $\omega^{(2)} > 0$) or in defocusing media with normal dispersion ($\chi > 0$, $\omega^{(2)} < 0$).

The damped motion is treated on the basis of the master equation

$$i\hbar \partial_t \hat{\rho} = [\hat{H}, \hat{\rho}] + i\gamma \hat{L} \hat{\rho}, \quad (4)$$

where

$$\gamma \hat{L} \hat{\rho} = \gamma \hbar \mathcal{A} \int dx \left[N_{\text{th}} (2\hat{a}^\dagger \hat{\rho} \hat{a} - \hat{\rho} \hat{a} \hat{a}^\dagger - \hat{a} \hat{a}^\dagger \hat{\rho}) + (N_{\text{th}} + 1) (2\hat{a} \hat{\rho} \hat{a}^\dagger - \hat{\rho} \hat{a}^\dagger \hat{a} - \hat{a}^\dagger \hat{a} \hat{\rho}) \right], \quad (5)$$

with γ being the damping constant, and

$$N_{\text{th}} = \left[\exp \left(\frac{\omega_c \hbar}{k_B T} \right) - 1 \right]^{-1} \quad (6)$$

(k_B - Boltzmann constant, T - temperature). The model applies to pulses longer than 1 ps, otherwise the influence of additional effects such as Raman scattering and third order dispersion must be taken into account.

The master equation (4) is converted, after spatial discretization, into a pseudo-Fokker-Planck equation for an s -parametrized multi-dimensional phase-space function, which is solved numerically using cumulant expansion in Gaussian approximation. The initial condition is realized by a multimode displaced thermal state, without internal entanglement, and it is assumed that the field expectation value corresponds to the classical fundamental soliton. In the numerical calculation, the coordinates x and t are scaled by the initial pulse width x_0 and the dispersion time $t_d = x_0^2 |\omega^{(2)}|^{-1}$ respectively. The calculations are performed on a grid of 200 points with discretization step $\Delta x = 0.1 x_0$ for an initial photon number of the pulse of $2\bar{n} = 2|\omega^{(2)}\mathcal{A}/(\chi x_0)| = 2 \cdot 10^9$ and a reservoir photon number of $N_{\text{th}} = 10^{-16}$. The value of N_{th} corresponds to a carrier wavelength of $\lambda_c = 2\pi c/\omega_c = 1.5 \mu\text{m}$ of the pulse in vacuum and a temperature of $T = 300\text{K}$ [see Eq. (6)]. Thus the pulse is initially prepared in a displaced thermal state that is almost a coherent state.

III. NONCLASSICAL SPECTRAL CORRELATIONS

In order to study spectral properties, bosonic operators in the Fourier space are introduced,

$$\hat{a}(\omega, t) = \frac{1}{\sqrt{2\pi}} \int_{-\infty}^{\infty} dx e^{i\omega x} \hat{a}(x, t). \quad (7)$$

The operator \hat{N}_i of the number of photons in a frequency interval (Ω_i, Ω'_i) , i.e., $\Omega_i \leq \omega \leq \Omega'_i$, reads

$$\hat{N}_i = \mathcal{A} \int_{\Omega_i}^{\Omega'_i} d\omega \hat{a}^\dagger(\omega, t) \hat{a}(\omega, t), \quad (8)$$

and the photon-number variance of the beam associated with this frequency interval can be given by

$$\langle \Delta \hat{N}_i^2 \rangle = \langle \hat{N}_i^2 \rangle - \langle \hat{N}_i \rangle^2 = \langle : \Delta \hat{N}_i^2 : \rangle + \langle \hat{N}_i \rangle, \quad (9)$$

where $: :$ introduces normal ordering. When the inequality

$$\langle : \Delta \hat{N}_i^2 : \rangle < 0 \quad (10)$$

is valid – a condition that cannot be satisfied within the classical noise theory – then sub-Poissonian statistics are observed, i.e., $\langle \Delta \hat{N}_i^2 \rangle < \langle \hat{N}_i \rangle$.

Let us now consider two nonoverlapping frequency intervals (Ω_i, Ω'_i) , $i = 1, 2$. A measure of the mutual correlation of the photon-number variances in the two frequency intervals is the correlation coefficient

$$\eta_{12} = \frac{\langle \Delta \hat{N}_1 \Delta \hat{N}_2 \rangle}{\sqrt{\langle \Delta \hat{N}_1^2 \rangle \langle \Delta \hat{N}_2^2 \rangle}}. \quad (11)$$

(note that $\langle \Delta \hat{N}_1 \Delta \hat{N}_2 \rangle = \langle : \Delta \hat{N}_1 \Delta \hat{N}_2 : \rangle$ for nonoverlapping frequency intervals). From the Cauchy-Schwarz inequality

$$\langle \Delta \hat{N}_1^2 \rangle \langle \Delta \hat{N}_2^2 \rangle - \langle \Delta \hat{N}_1 \Delta \hat{N}_2 \rangle^2 \geq 0 \quad (12)$$

it follows that the absolute value of the correlation coefficient is limited to the right,

$$|\eta_{12}| \leq 1. \quad (13)$$

Obviously, the correlation is nonclassical, if the inequality (12) is violated for normally ordered quantities, i.e.,

$$\langle : \Delta \hat{N}_1^2 : \rangle \langle : \Delta \hat{N}_2^2 : \rangle - \langle : \Delta \hat{N}_1 \Delta \hat{N}_2 : \rangle^2 < 0. \quad (14)$$

In order to give a quantitative measure of the degree of nonclassical correlation, we define the generalized correlation coefficient

$$\begin{aligned}\tilde{\eta}_{12} &= \frac{\langle : \Delta \hat{N}_1^2 : \rangle \langle : \Delta \hat{N}_2^2 : \rangle - \langle : \Delta \hat{N}_1 \Delta \hat{N}_2 : \rangle^2}{\left| \langle : \Delta \hat{N}_1^2 : \rangle \langle : \Delta \hat{N}_2^2 : \rangle - \langle : \Delta \hat{N}_1^2 : \rangle \langle : \Delta \hat{N}_2^2 : \rangle \right|} \\ &= \frac{\eta_{11}\eta_{22} - \eta_{12}^2}{|1 - \eta_{11}\eta_{22}|}\end{aligned}\quad (15)$$

where

$$\eta_{ii} = \frac{\langle : \Delta \hat{N}_i^2 : \rangle}{\langle : \Delta \hat{N}_i^2 : \rangle} \leq 1. \quad (16)$$

Note that η_{ii} is negative (positive) for sub-Poissonian (super-Poissonian) statistics. Nonclassical correlation is observed if

$$\tilde{\eta}_{12} < 0, \quad (17)$$

and it is easily proved that

$$\tilde{\eta}_{12} \geq -1. \quad (18)$$

From Eq. (15) it is easily seen that when

$$\langle : \Delta \hat{N}_1^2 : \rangle \langle : \Delta \hat{N}_2^2 : \rangle < 0, \quad (19)$$

then the correlation of the photon-number variances is nonclassical. Note that for Gaussian quantum states the criterion (14) is closely related to that used in [16].

Similarly, the mutual correlation of the numbers of photons in the two frequency intervals can be considered,

$$\tau_{12} = \frac{\langle \hat{N}_1 \hat{N}_2 \rangle}{\sqrt{\langle \hat{N}_1^2 \rangle \langle \hat{N}_2^2 \rangle}} \quad (20)$$

($|\tau_{12}| \leq 1$). Nonclassical correlation is realized if

$$\langle : \hat{N}_1^2 : \rangle \langle : \hat{N}_2^2 : \rangle - \langle : \hat{N}_1 \hat{N}_2 : \rangle^2 < 0, \quad (21)$$

or equivalently

$$\tilde{\tau}_{12} < 0, \quad (22)$$

with

$$\tilde{\tau}_{12} = \frac{\langle : \hat{N}_1^2 : \rangle \langle : \hat{N}_2^2 : \rangle - \langle : \hat{N}_1 \hat{N}_2 : \rangle^2}{\langle \hat{N}_1^2 \rangle \langle \hat{N}_2^2 \rangle - \langle : \hat{N}_1^2 : \rangle \langle : \hat{N}_2^2 : \rangle} \quad (23)$$

($\tilde{\tau}_{12} \geq -1$). Note that for the photon numbers an inequality analogous to (19) is not valid, since the average of the normally ordered square of a photon number cannot be negative.

The spectral photon-number statistics can be determined using a setup shown in Fig. 1. The scheme in Fig. 1(a) is used in [13] (and with slightly modified detection in [14]) for measuring spectral photon-number squeezing. The scheme can also be used to reconstruct correlations between different spectral components from the measured data [16]. However with regard to direct correlation measurement, a scheme of the type shown in Fig. 1(b) may be better suited for that purpose. Omitting the detectors, the schemes can also be used for selecting from the original beam partial beams that are highly nonclassical.

IV. RESULTS

A. Narrow bandwidth intervals

In Fig. 2 the temporal evolution of the coefficient η_{11} , Eq.(16), is plotted for a narrow bandwidth mid-interval $(\Omega_1, \Omega'_1) = (-\Delta\omega, \Delta\omega)$, $\Delta\omega/\omega_0 \ll 1$, and various values of the damping parameter γ (here and in the following frequencies are scaled by $\omega_0 = x_0^{-1}$ [35]). The strongest sub-Poissonian effect is observed for $\gamma t_d = 0.03$ at $t \sim 10t_d$. Surprisingly, the sub-Poissonian statistics of the narrow bandwidth mid-component can be stronger for a damped soliton than for the undamped one [34]. The temporal evolution of the coefficient η_{11} as a function of the frequency ω [for a narrow bandwidth interval $(\Omega_1, \Omega'_1) = (\omega - \Delta\omega, \omega + \Delta\omega)$] is plotted in Fig. 3 for (a) $\gamma = 0$ and (b) $\gamma t_d = 0.03$. From the figure it is seen that the interference pattern which is typically obtained in the limit of vanishing absorption [Fig. 3(a)] is not observed for an absorbing fiber [Fig. 3(b)]. Note that in the limit of vanishing absorption the results obtained here are in good agreement with those obtained by stochastic simulations within the frame of the positive P representation [33].

Disregarding absorption and solving the cumulant evolution equations given in [34] in a linearization approximation, the solution can be given by eigenfunction expansion, the expansion coefficients being determined by the chosen initial condition. The result of superposition then corresponds to an interference pattern like that in Fig. 3(a). Obviously, the (phase-sensitive) terms that are superimposed do not respond uniformly to absorption, so that the internal coherences responsible for the interference pattern can be destroyed at least in part. In particular, near the center of the spectrum ($\omega \rightarrow 0$) the super-Poissonian peaks are fully suppressed and in place of them sub-Poissonian statistics is observed. Accordingly, the super-Poissonian side-band formation that appears with increasing frequency is more uniform for an absorbing fiber than for a nonabsorbing one.

To get an insight into the correlation between spectral components at different frequencies ω_1 and ω_2 [for narrow bandwidth intervals $(\Omega_i, \Omega'_i) = (\omega_i - \Delta\omega, \omega_i + \Delta\omega)$, $i = 1, 2$], we have plotted the correlation coefficients η_{12} [Eq. (11), Fig. 4], $\tilde{\eta}_{12}$ [Eq. (15), Fig. 5], and $\tilde{\tau}_{12}$ [Eq. (23), Fig. 6] as functions of ω_1 and ω_2 for $\gamma = 0$ and $\gamma t_d = 0.03$, restricting our attention to the two characteristic propagation times $t = 5t_d$ and $t = 10t_d$ (cf. Fig. 3). Figures 4(a) and 4(b) reveal that the super-Poissonian side-band components observed at the propagation time $t = 5t_d$ (Fig. 3) are strongly positively correlated with respect to the photon-number variance, whereas relatively strong negative correlation between the super-Poissonian side-band

components and the sub-Poissonian mid-components is observed – effects which can be found for both a nonabsorbing fiber, Fig. 4(a), and an absorbing fiber, Fig. 4(b). The notably reduced correlation observed at the propagation time $t = 10 t_d$ for a nonabsorbing fiber, Fig. 4(c), may be viewed as an interference effect in a similar sense as mentioned above. From that it can be understood that absorption can enhance correlation – a surprising effect which can be seen from Fig. 4(d).

From Fig. 5 it is seen that nonclassical correlation of the photon-number variance appears between sideband super-Poissonian components and – in agreement with the condition (19) – between the sub-Poissonian mid-component and the super-Poissonian sideband components. The relatively strong nonclassical correlation $\tilde{\eta}_{12} \sim -7.3 \cdot 10^{-3}$ observed for a nonabsorbing fiber at the propagation time $t = 5 t_d$ [Fig. 5(a)] reduces to $\tilde{\eta}_{12} \sim -8.6 \cdot 10^{-4}$ at $t = 10 t_d$ [Fig. 5(c)]. The behavior of $\tilde{\eta}_{12}$ for an absorbing fiber may be quite different, as is seen from comparison of Figs. 5(a) and 5(c) with Figs. 5(b) and 5(d), respectively. Whereas at $t = 5 t_d$ the effect of nonclassical correlation is weaker, $\tilde{\eta}_{12} \sim -3 \cdot 10^{-3}$ [Fig. 5(b)], a stronger effect is observed at $t = 10 t_d$, $\tilde{\eta}_{12} \sim -4.8 \cdot 10^{-3}$ [Fig. 5(d)]. The latter reflects the enhanced correlation between the mid-component and the sideband components as shown in Fig. 4(d). We are again left with the surprising fact that absorption can enhance nonclassical behavior.

Figure 6 shows that the photon-number correlation can be quite different from the correlation of the photon-number variance. Contrary to the photon-number variance, there is no nonclassical correlation of the photon numbers of the sub-Poissonian mid-component and the super-Poissonian sideband components, since for the photon number an inequality of the type (19) cannot be valid. Nevertheless, the minimum value $\tilde{\tau}_{12} \sim -0.02$ obtained for a nonabsorbing fiber at the propagation time $t = 5 t_d$ [Fig. 6(a)] is smaller than the minimum value $\tilde{\eta}_{12} \sim -7.3 \cdot 10^{-3}$ [Fig. 5(a)], and hence a stronger nonclassical correlation is observed for the photon number than the photon-number variance. Moreover, the effect of nonclassical correlation observed at the propagation time $t = 10 t_d$ is weaker than that at $t = 5 t_d$ for both a nonabsorbing fiber [Fig. 6(c)] and an absorbing one [Fig. 6(d)] [contrary to the correlation of the photon-number variance, Fig. 5(b) and (d)].

B. Finite bandwidth intervals

Let us return to the coefficient η_{11} . Allowing for finite frequency windows, we consider a frequency interval $(\Omega_1, \Omega'_1) = (-\Omega, \Omega)$ [for the scheme, see Fig. 1(a)] and optimize Ω such that the sub-Poissonian components dominates the signal and η_{11} becomes minimal for all times (Fig. 7). From Fig. 7(d) it is seen that for a nonabsorbing fiber the absolute minimum of η_{11} that is attainable in

this way is $\eta_{11} \sim -3.5$ ($t \sim 4.5 t_d$), which corresponds to a Fano factor of $F_1 = \langle \Delta \hat{N}_1^2 \rangle / \langle \hat{N}_1 \rangle = (1 - \eta_{11})^{-1} \sim 0.23$ or ~ 6.4 dB squeezing (cf. [30,36]). In that case $\sim 80\%$ of the photons of the initial, full pulse contribute to the filtered pulse [Fig. 7(c)]. It is further seen that the oscillating behavior of η_{11} as a function of the propagation time is damped out owing to absorption such that for certain propagation times stronger sub-Poissonian statistics can be observed for an absorbing fiber than a nonabsorbing one. This effect is of course a consequence of the behavior of the narrow bandwidth components as addressed in Sec. IV A. The observed discrepancy between Ω [Fig. 7(a)] and Ω_0 [Fig. 7(b), for the definition of Ω_0 , see Fig. 3], e.g., for $\gamma t_d = 0 \dots 0.005$ at $t \gtrsim 9 t_d$, obviously results from the correlation between different frequency components (cf. [13,30]).

To obtain strong nonclassical correlation between different beams, we first consider two (with respect to the center of the spectrum) symmetric frequency windows (Ω_1, Ω'_1) and $(\Omega_2, \Omega'_2) = (-\Omega'_1, -\Omega_1)$ [for the scheme, see Fig. 1(b)] and optimize Ω_1 and Ω'_1 such that $\tilde{\eta}_{12}$ (Fig. 8) and $\tilde{\tau}_{12}$ (Fig. 9) become minimal. From inspection of Fig. 8(d) the absolute minimum of $\tilde{\eta}_{12}$ is realized for a nonabsorbing fiber ($\tilde{\eta}_{12} \sim -0.48$ at $t \sim 4.5 t_d$). The effect of absorption is again seen to damp out the oscillations of $\tilde{\eta}_{12}$ (as a function of the propagation time) such that at certain propagation times [$\gamma t_d = 0.01 \dots 0.02$, $t/t_d = 6 \dots 14$ in Fig. 8(d)] stronger nonclassical correlation can be achieved for an absorbing fiber than a nonabsorbing one. On the contrary, Fig. 9(d) reveals that dissipation always reduces the nonclassical photon-number correlation, i.e., for any propagation time the lower bound of the coefficient $\tilde{\tau}_{12}$ is realized in the limit of vanishing absorption. Note that the strongest nonclassical photon-number correlation ($\tilde{\tau}_{12} = -0.32$ at $t \sim 3.5 t_d$) is weaker than the strongest nonclassical correlation of the photon-number variance.

For weak absorption ($\gamma t_d = 0 \dots 0.005$) from Figs. 8(a) and (b) a (quasi-)periodic change of the frequency interval (Ω_1, Ω'_1) is seen, in agreement with the results in Sec. IV A. At the early stage of propagation the frequency interval is essentially determined by the nonclassically correlated super-Poissonian sideband components. Later [at $t \sim 3 t_d$ in Figs. 8(a) and (b)] it shifts towards the mid-frequency, which indicates the increasing weight of the sub-Poissonian mid-components. The shift back to the sideband components obviously results from the (quasi-)periodic formation of super-Poissonian (and sub-Poissonian) components in the center of the spectrum [cf. Fig. 3(a)]. The fraction of the number of photons in each beam relative to the number of photons in the initial, full beam changes from less than 5% for sideband frequency windows to about 40% for near mid-frequency windows [Fig. 8(c)]. With increasing absorption only the first shift of the frequency window from the sideband to the central part is observed. In contrast to $\tilde{\eta}_{12}$, minimization of $\tilde{\tau}_{12}$ always requires sideband frequency windows [Figs. 9(a)

and (b)], where each beam contains less than 10% of the initial number of pulse photons [Fig. 9(c)].

Whereas symmetric windows are expected to be best suited to realization of minimal $\tilde{\tau}_{12}$, from Fig. 5 it is suggested that asymmetric windows may be more suited to realization of minimal $\tilde{\eta}_{12}$. This is fully confirmed by the calculation. The symmetric windows shown in Fig. 9 indeed yield the smallest value of $\tilde{\tau}_{12}$. A comparison of Fig. 8(d) with Fig. 10 reveals that $\tilde{\eta}_{12}$ can be reduced if asymmetric windows are used. In particular, it is seen that the absolute minimum of $\tilde{\eta}_{12}$ observed for a nonabsorbing fiber can be reduced to $\tilde{\eta}_{12} \sim -0.71$ ($t \sim 5.5t_d$). A more detailed analysis is given in Fig. 11. It is seen that only at a early stage of propagation symmetric and asymmetric frequency windows yield equal values of $\tilde{\eta}_{12}$. Obviously, asymmetric frequency windows take better account of the nonclassical correlation between sub-Poissonian mid-components and super-Poissonian sideband components in order to reduce $\tilde{\eta}_{12}$. The price to be paid are the unequal photon numbers of the two beams, since the number of photons in the spectral interval around the center is substantially larger than that in the sideband interval, as is seen from the figure. Hence for generation of (with respect to the photon-number variance) nonclassically correlated beams, the frequency windows should be chosen such that an optimum between nonclassical correlation and beam intensities is observed.

V. SUMMARY AND CONCLUDING REMARKS

We have studied the internal quantum statistics of fundamental solitons in absorbing Kerr media, applying multimode cumulant-expansion techniques and solving the resulting evolution equations numerically in Gaussian approximation. In particular, we have calculated the temporal evolution of the photon-number variance, its correlation, and the photon-number correlation for various frequency windows. The formation of super-Poissonian side-

band components with nonclassically correlated photon numbers and nonclassically correlated photon-number variances may be regarded as being a typical signature of the quantum nature of a soliton pulse.

Since a soliton pulse is a highly involved multimode field, interference effects can essentially determine its properties. It is worth noting that absorption can damp out interferences that are destructive with respect to nonclassical features, such as squeezing and the nonclassical correlations mentioned, so that absorption surprisingly improves, under certain conditions, these nonclassical effects. The calculations show that for a nonabsorbing fiber propagation distances of $3.5 \dots 5.5$ dispersion lengths are best suited for detecting the nonclassical features. Destructive interferences are observed at distances of $8 \dots 12$ dispersion lengths. At these distances the best values for photon-number squeezing and nonclassical correlation of the photon-number variance are achieved for an absorbing fiber ($\gamma t_d \sim 0.02$).

Using appropriately chosen spectral windows, a soliton pulse can serve as a source of nonclassically correlated light beams. We have considered both symmetric and asymmetric windows and optimized them such that the filtered beams are maximally nonclassically correlated with regard to the photon number and the photon-number variance. It should be pointed out that in practice a number of effects such as Raman scattering and third-order dispersion should be included in a refined theoretical model. Finally, inclusion in the calculation of non-Gaussian effects for weak absorption has been a challenge.

ACKNOWLEDGMENTS

This work was supported by the Deutsche Forschungsgemeinschaft. We are grateful to F. König, G. Leuchs, and A. Sizmann for valuable discussions.

[1] P. D. Drummond, R. M. Shelby, S. R. Friberg, and Y. Yamamoto, *Nature* (London) **365**, 307 (1993).
[2] A. Sizmann, *Appl. Phys. B* **65**, 745 (1997).
[3] M. E. Anderson, D. F. McAlister, M. G. Raymer, and M. C. Gupta, *J. Opt. Soc. Am. B* **14**, 3180 (1997).
[4] I. Abram, *Physics World* **12**, 21 (1999).
[5] A. Hasegawa, *Optical Solitons in Fibers* (Springer-Verlag, Berlin, 1989).
[6] S. A. Akhmanov, V. A. Vysloukh, and A. S. Chirkin, *Optics of Femtosecond Laser Pulses* (AIP, New York, 1992).
[7] M. Kitagawa and Y. Yamamoto, *Phys. Rev. A* **34**, 3974 (1986).
[8] S. R. Friberg, S. Machida, and Y. Yamamoto, *Phys. Rev. Lett.* **69**, 3165 (1992).
[9] S. Späler, P. van Loock, A. Sizmann, and G. Leuchs, *Appl. Phys. B* **64**, 213 (1997).
[10] J.-M. Courty *et al.*, *Phys. Rev. A* **58**, 1501 (1998).
[11] M. Rosenbluh and R. M. Shelby, *Phys. Rev. Lett.* **66**, 153 (1991).
[12] K. Bergman, H. A. Haus, E. I. Ippen, and M. Shirasaki, *Opt. Lett.* **19**, 290 (1994).

- [13] S. R. Friberg *et al.*, Phys. Rev. Lett. **77**, 3775 (1996).
- [14] S. Spälter *et al.*, Europhys. Lett. **38**, 335 (1997).
- [15] S. Schmitt *et al.*, Phys. Rev. Lett. **81**, 2446 (1998).
- [16] S. Spälter *et al.*, Phys. Rev. Lett. **81**, 786 (1998).
- [17] Y. Lai and H. A. Haus, Phys. Rev. A **40**, 854 (1989).
- [18] D. Yao, Phys. Rev. A **52**, 1574 (1995).
- [19] F. X. Kärtner and L. Boivin, Phys. Rev. A **53**, 454 (1996).
- [20] Y. Lai and H. A. Haus, Phys. Rev. A **40**, 844 (1989).
- [21] F. Singer, M. J. Potasek, J. M. Fang, and M. C. Teich, Phys. Rev. A **46**, 4192 (1992).
- [22] H. A. Haus and Y. Lai, J. Opt. Soc. Am. B **7**, 386 (1990).
- [23] Y. Lai and H. A. Haus, Phys. Rev. A **42**, 2925 (1990).
- [24] Y. Lai, J. Opt. Soc. Am. B **10**, 475 (1993).
- [25] C. R. Doerr, M. Shirasaki, and F. I. Khatri, J. Opt. Soc. Am. B **11**, 143 (1994).
- [26] Y. Lai and S.-C. Yu, Phys. Rev. A **51**, 817 (1995).
- [27] P. D. Drummond and S. J. Carter, J. Opt. Soc. Am. B **4**, 1565 (1987).
- [28] P. D. Drummond and A. D. Hardman, Europhys. Lett. **21**, 279 (1993).
- [29] S. J. Carter, Phys. Rev. A **51**, 3274 (1995).
- [30] M. J. Werner, Phys. Rev. A **54**, R2567 (1996).
- [31] M. J. Werner and P. D. Drummond, Phys. Rev. A **56**, 1508 (1997).
- [32] M. J. Werner and P. D. Drummond, J. Comput. Phys. **132**, 312 (1997).
- [33] M. J. Werner and S. R. Friberg, Phys. Rev. Lett. **79**, 4143 (1997).
- [34] E. Schmidt, L. Knöll, and D.-G. Welsch, Phys. Rev. A **59**, 2442 (1999).
- [35] The frequency scaling in [34] should read $\omega_0 = 2/x_0$, so that $\omega_{\max} = \pi/\Delta x = 5\pi\omega_0$ and $\Delta\omega_{\min} = 2\pi/(m\Delta x) = 0.05\pi\omega_0$ for the chosen values of $\Delta x = 0.1x_0$ and $m = 200$.
- [36] A. Mecozzi and P. Kumar, Opt. Commun. **22**, 1232 (1997).

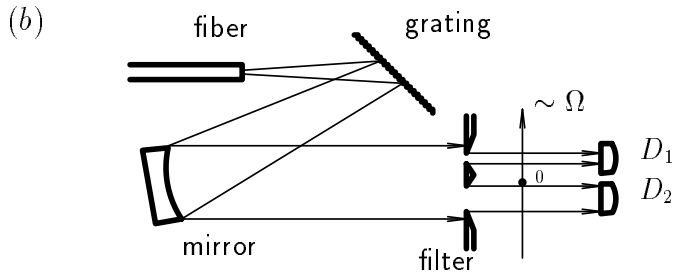
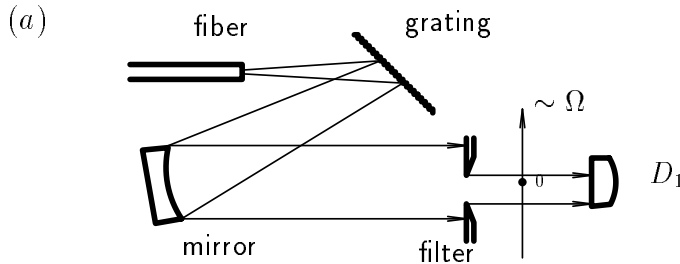


FIG. 1. Experimental setup for studying the spectrally resolved quantum statistics of soliton pulses. The scheme (a) is suited for measurement of the photon-number statistics [13,14], whereas the scheme (b) allows one to perform correlation measurements. If the detectors D_1 and D_2 are omitted, the schemes can be used for selecting from the original beam partial beams that are highly nonclassical.

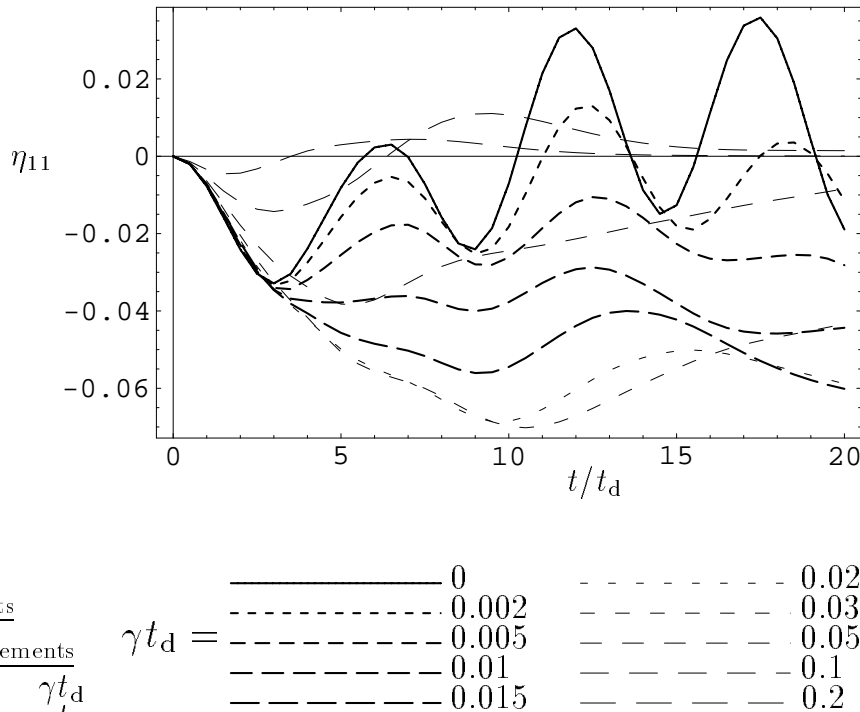
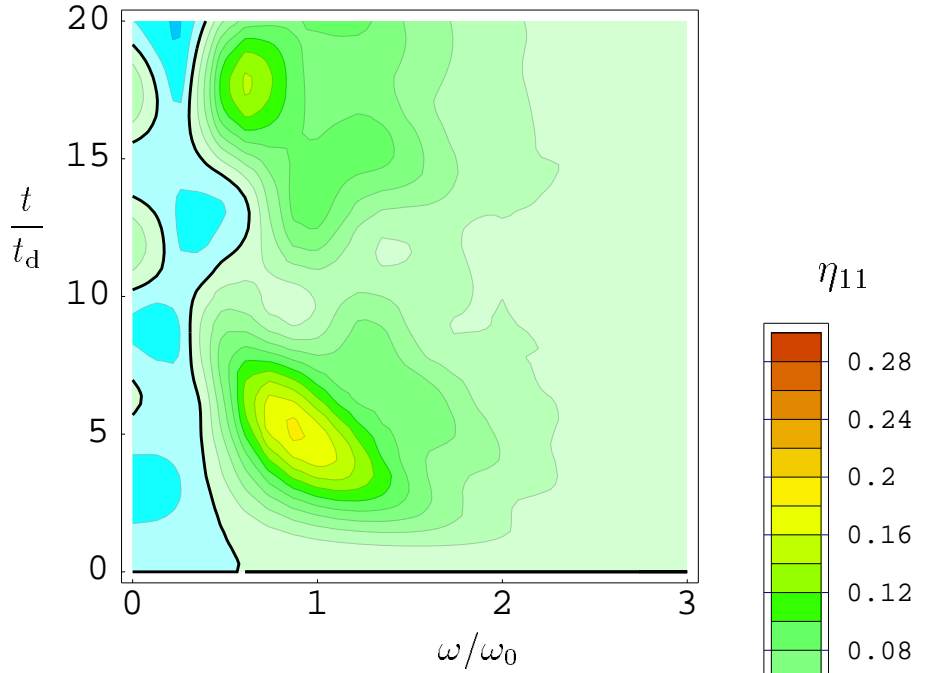


FIG. 2. The temporal evolution of the coefficient η_{11} , Eq. (16), is shown for the spectral interval $(\Omega_1, \Omega'_1) = (-\Delta\omega, \Delta\omega)$, $\Delta\omega = 0.05\pi\omega_0$, and various values of the damping parameter γ .

(a) $\gamma = 0$



(b) $\gamma t_d = 0.03$

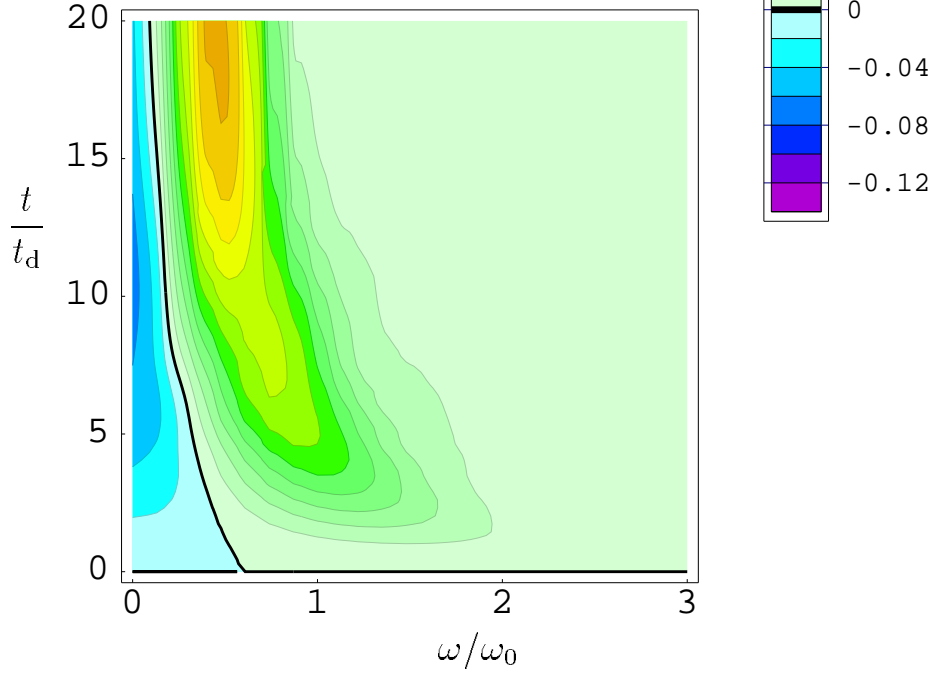
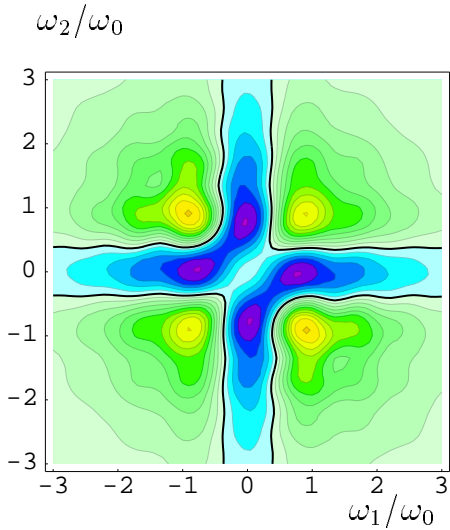
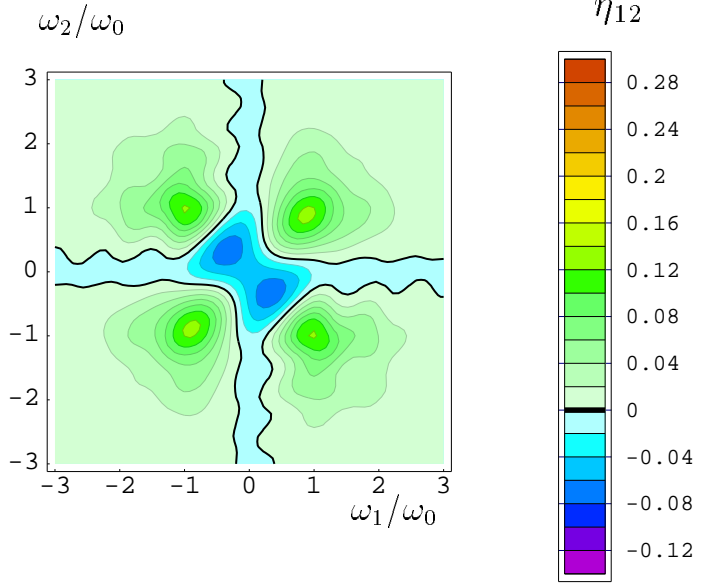


FIG. 3. The temporal evolution of the coefficient η_{11} , Eq. (16), is shown as a function of the frequency ω for the spectral interval $(\Omega_1, \Omega'_1) = (\omega - \Delta\omega, \omega + \Delta\omega)$, $\Delta\omega = 0.05\pi\omega_0$, and the damping parameter $\gamma = 0.03/t_d$. Note that η_{11} is an even function of ω . The thick solid line from the bottom to the top defines the frequency Ω_0 [used in Fig. 7(b)] such that $\eta_{11} > 0$ for $|\omega| > \Omega_0$.

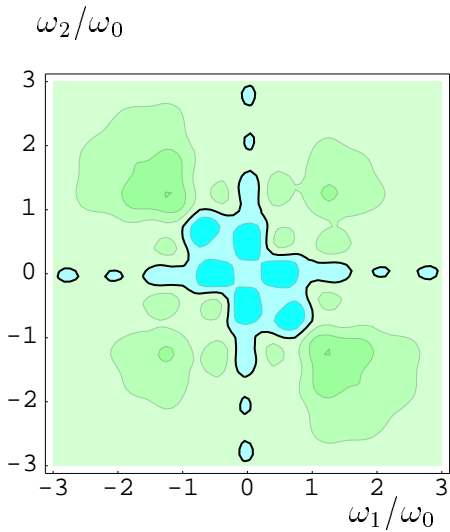
(a) $\gamma = 0, t = 5 t_d$



(b) $\gamma t_d = 0.03, t = 5 t_d$



(c) $\gamma = 0, t = 10 t_d$



(d) $\gamma t_d = 0.03, t = 10 t_d$

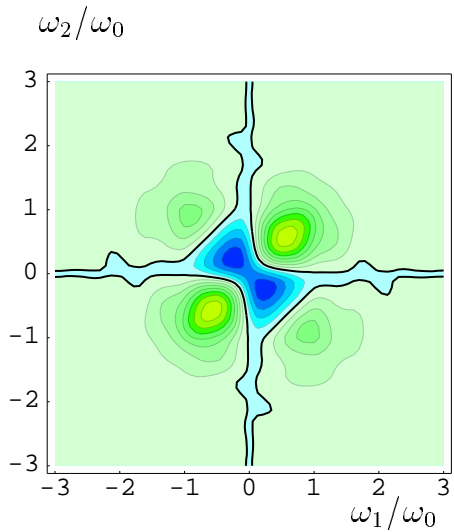
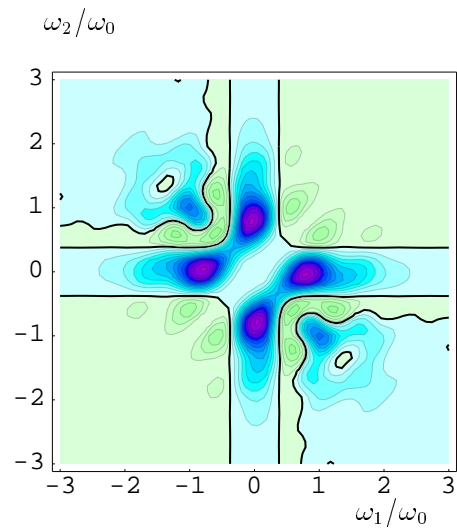
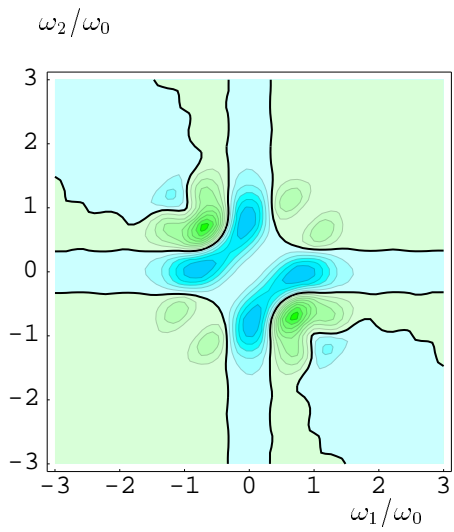


FIG. 4. The correlation coefficient η_{12} , Eq. (11), is shown as a function of the frequencies ω_i for the spectral intervals $(\Omega_i, \Omega'_i) = (\omega_i - \Delta\omega, \omega_i + \Delta\omega)$, $\Delta\omega = 0.05\pi\omega_0$ ($i = 1, 2$), and (a) $\gamma = 0, t = 5 t_d$, (b) $\gamma = 0.03/t_d, t = 5 t_d$, (c) $\gamma = 0, t = 10 t_d$, (d) $\gamma = 0.03/t_d, t = 10 t_d$.

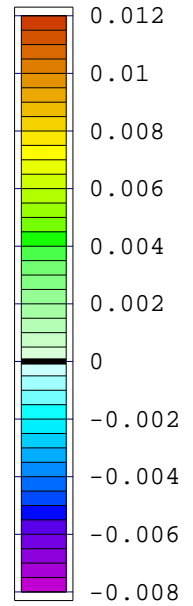
(a) $\gamma = 0, t = 5 t_d$



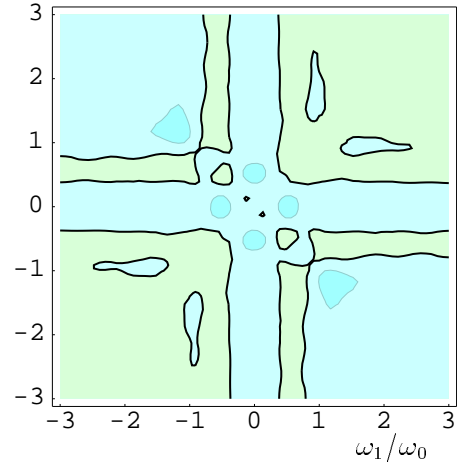
(b) $\gamma t_d = 0.03, t = 5 t_d$



$\tilde{\eta}_{12}$



(c) $\gamma = 0, t = 10 t_d$



(d) $\gamma t_d = 0.03, t = 10 t_d$

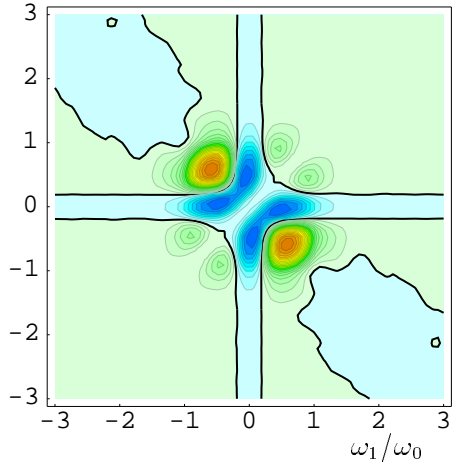
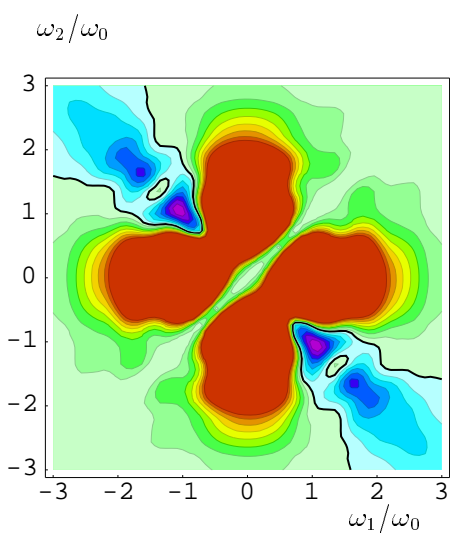
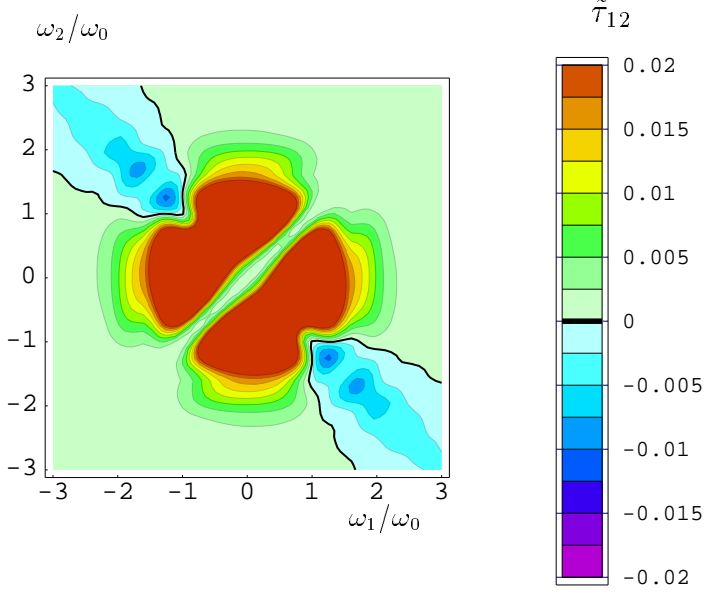


FIG. 5. The coefficient $\tilde{\eta}_{12}$, Eq. (15), is shown as a function of the frequencies ω_i for the spectral intervals $(\Omega_i, \Omega'_i) = (\omega_i - \Delta\omega, \omega_i + \Delta\omega)$, $\Delta\omega = 0.05\pi\omega_0$ ($i=1, 2$), and (a) $\gamma = 0, t = 5 t_d$, (b) $\gamma = 0.03/t_d, t = 5 t_d$, (c) $\gamma = 0, t = 10 t_d$, (d) $\gamma = 0.03/t_d, t = 10 t_d$. Negative values of $\tilde{\eta}_{12}$ indicate nonclassical correlation of the photon-number variances at chosen frequencies ω_1 and ω_2 .

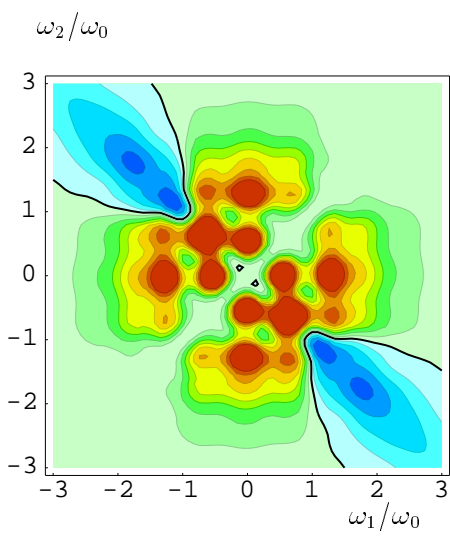
(a) $\gamma = 0, t = 5 t_d$



(b) $\gamma t_d = 0.03, t = 5 t_d$



(c) $\gamma = 0, t = 10 t_d$



(d) $\gamma t_d = 0.03, t = 10 t_d$

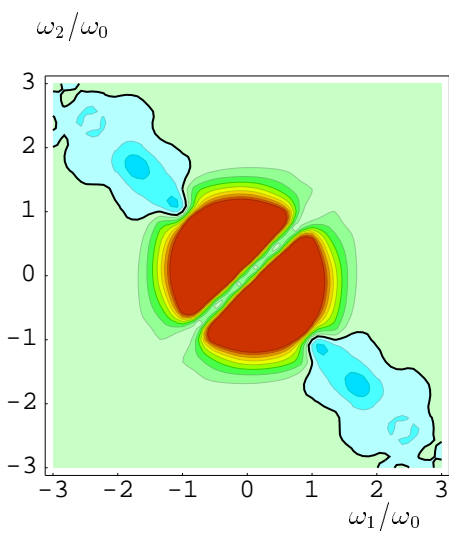


FIG. 6. The coefficient $\tilde{\tau}_{12}$, Eq. (23), is shown as a function of the frequencies ω_i for the spectral intervals $(\Omega_i, \Omega'_i) = (\omega_i - \Delta\omega, \omega_i + \Delta\omega)$, $\Delta\omega = 0.05\pi\omega_0$ ($i = 1, 2$), and (a) $\gamma = 0, t = 5 t_d$, (b) $\gamma t_d = 0.03/t_d, t = 5 t_d$, (c) $\gamma = 0, t = 10 t_d$, (d) $\gamma t_d = 0.03/t_d, t = 10 t_d$. Values $\tilde{\tau}_{12} > 0.02$ are not depicted. Negative values of $\tilde{\tau}_{12}$ indicate nonclassical correlation of the photon numbers at chosen frequencies ω_1 and ω_2 .

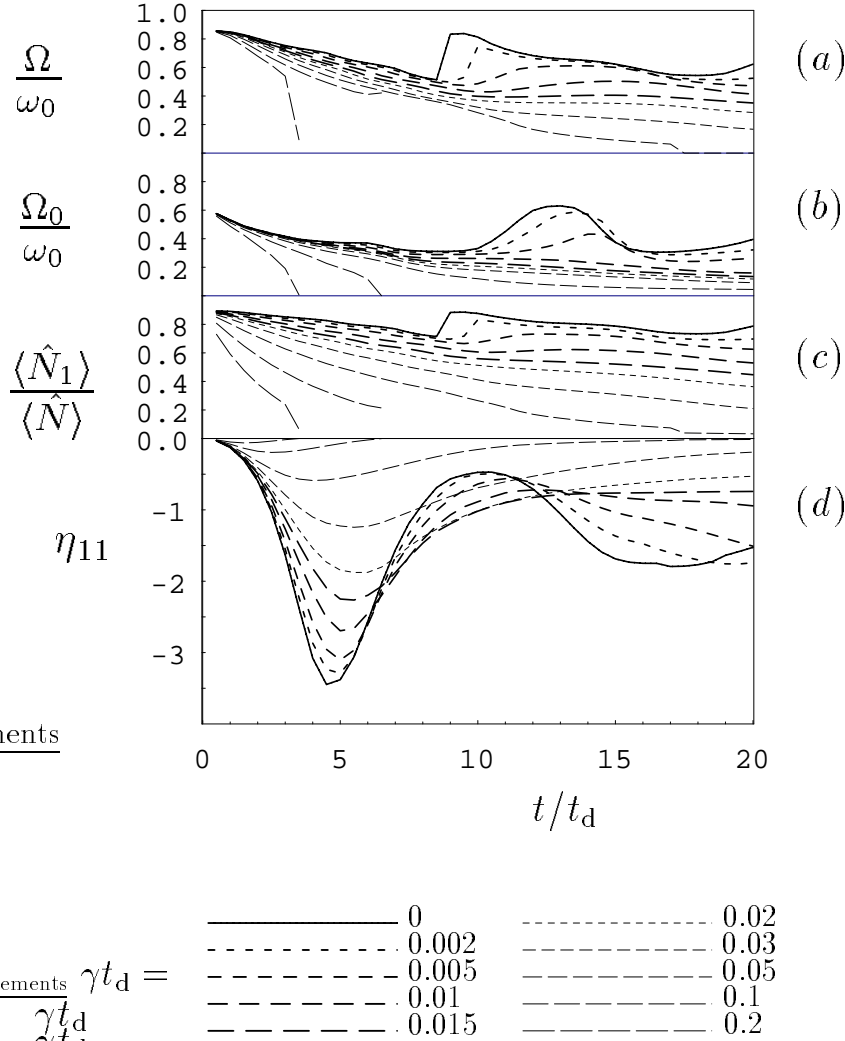


FIG. 7. Optimization of the square bandpass filter [Fig.1(a)] for realization of maximum sub-Poissonian statistics. The temporal evolution of (a) the spectral interval $(\Omega_1, \Omega'_1) = (-\Omega, \Omega)$, (c) the number $\langle \hat{N}_1 \rangle$ of photons ($\langle \hat{N} \rangle$ is the total number of photons in the initial pulse), and (d) the minimum value of the coefficient η_{11} , Eq. (16), for that interval are shown for various values of the damping parameter γ . For comparison (b), the frequency Ω_0 defined in Fig. 3 is shown.

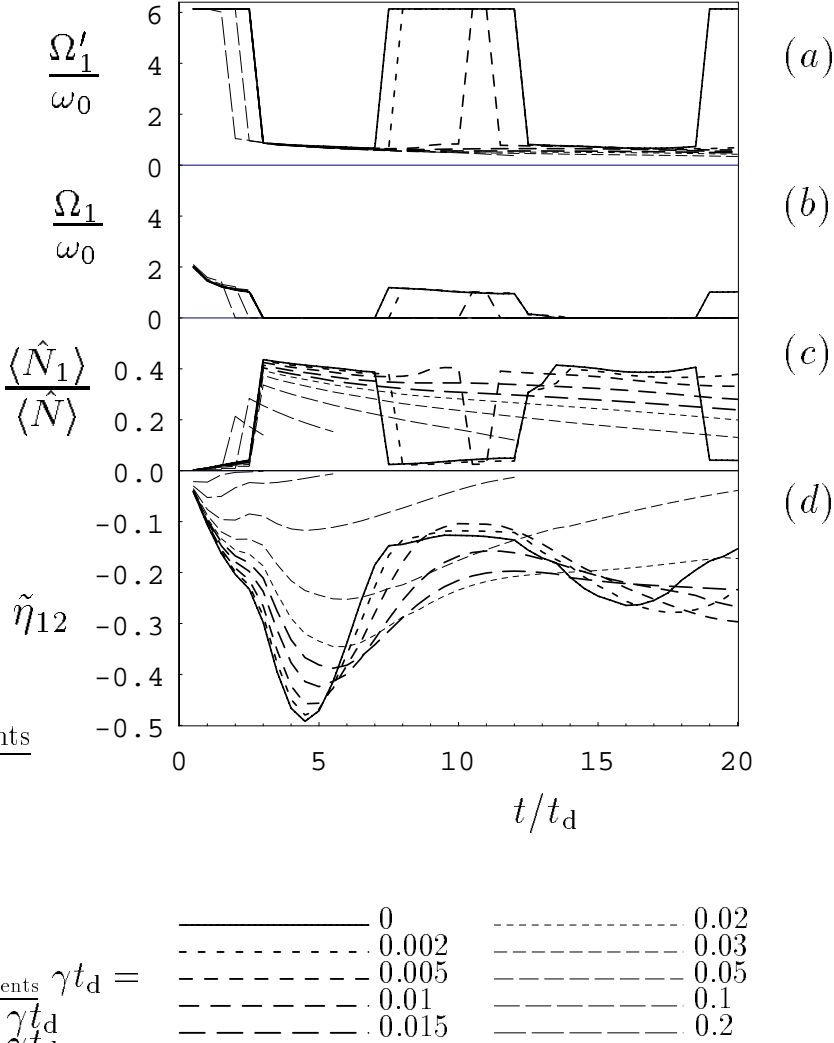


FIG. 8. Optimization of two (with respect to the center of the spectrum) symmetric square bandpass filters [Fig. 1(b)] for realization of strong nonclassical correlation of the photon-number variance between the selected beams. The temporal evolution of (a), (b) the spectral interval (Ω_1, Ω'_1) , (c) the number $\langle \hat{N}_1 \rangle$ of photons in a beam ($\langle \hat{N} \rangle$ is the total number of photons in the initial pulse), and (d) the minimum value of the coefficient $\tilde{\eta}_{12}$, Eq. (15), are shown for various values of the damping parameter γ .

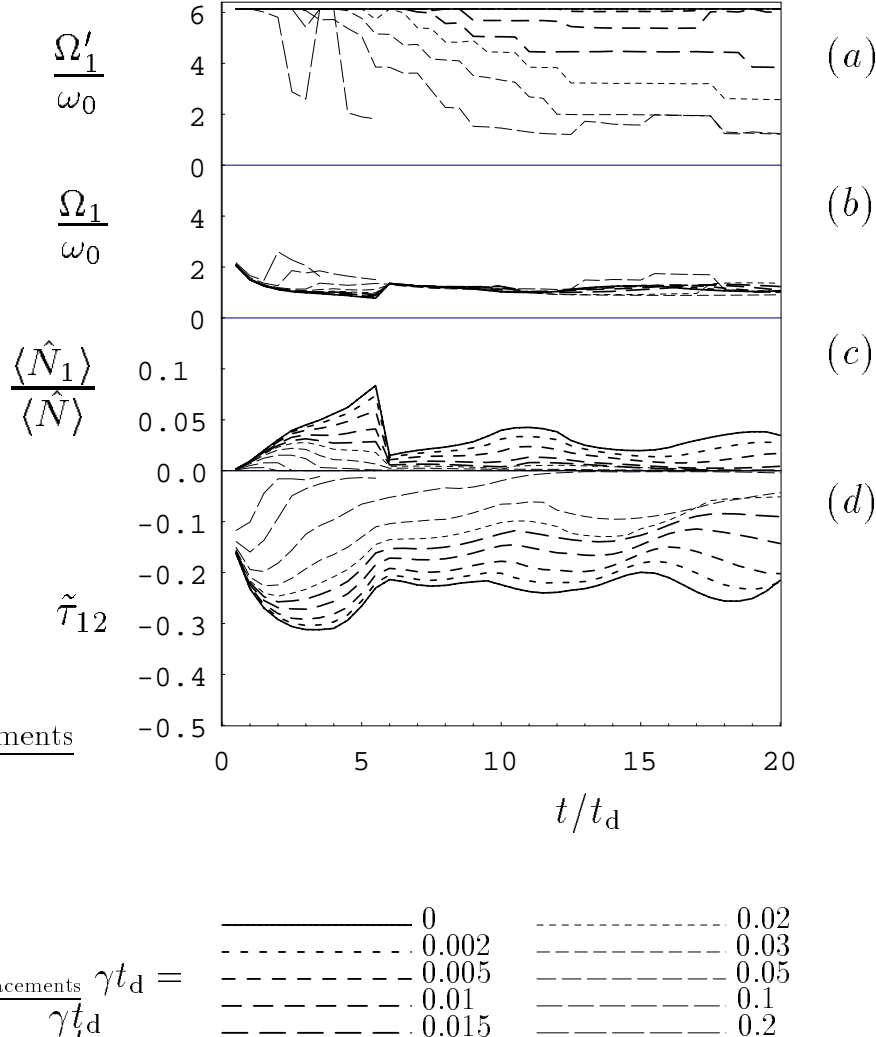


FIG. 9. Optimization of two (with respect to the center of the spectrum) symmetric square bandpass filters [Fig. 1(b)] for realization of strong nonclassical photon-number correlation between the selected beams. The temporal evolution of (a), (b) the spectral interval (Ω_1, Ω'_1) , (c) the number $\langle \hat{N}_1 \rangle$ of photons in a beam ($\langle \hat{N} \rangle$ is the total number of photons in the initial pulse), and (d) the minimum value of the coefficient $\tilde{\tau}_{12}$, Eq. (23), are shown for various values of the damping parameter γ .

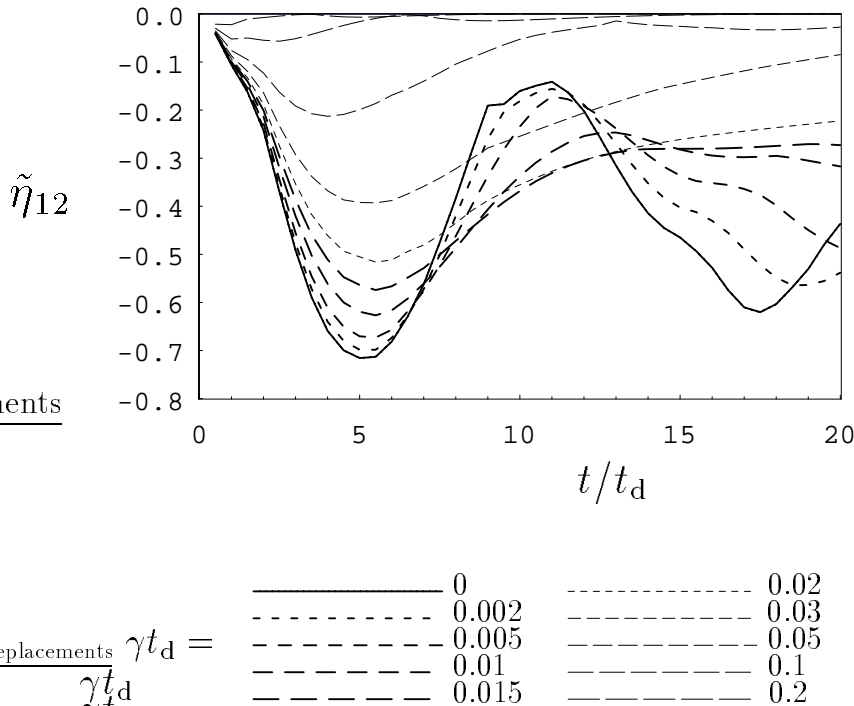


FIG. 10. The temporal evolution of the minimum value of the coefficient $\tilde{\eta}_{12}$, Eq. (15), attainable for two beams obtained from asymmetric (nonoverlapping) frequency windows (Ω_i, Ω'_i) , $i = 1, 2$, is shown for various values of the damping parameter γ .

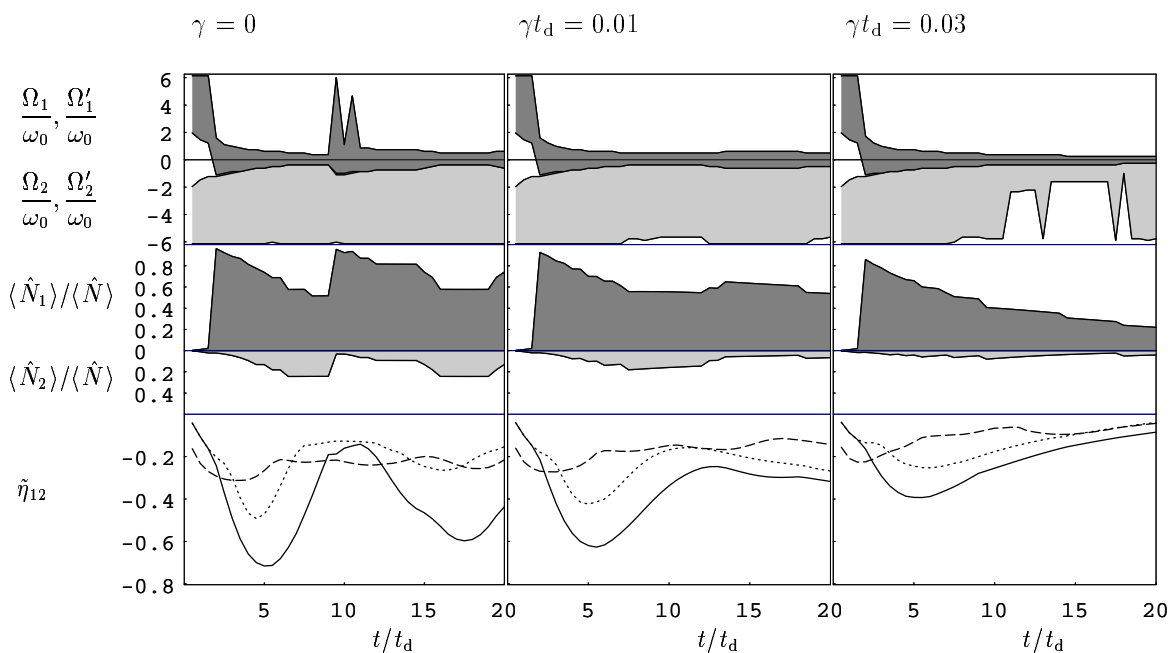


FIG. 11. Optimization of two (with respect to the center of the spectrum) unsymmetric square bandpass filters [Fig. 1(b)] for realization of strong nonclassical correlation of the photon-number variance between the selected beams. The temporal evolution of the spectral intervals (Ω_i, Ω'_i) , $i = 1, 2$, the numbers $\langle \hat{N}_i \rangle$ of photons in the beams ($\langle \hat{N} \rangle$ is the total number of photons in the initial pulse), and the minimum value of the coefficient $\tilde{\eta}_{12}$, Eq. (15), are shown for (a) $\gamma = 0$, (b) $\gamma = 0.01/t_d$, (c) $\gamma = 0.03/t_d$. For comparison, the dotted line shows the minimum value of $\tilde{\eta}_{12}$ obtained for symmetric windows as given in Fig. 8, and the dashed line shows the minimum value of $\tilde{\tau}_{12}$ as given in Fig. 9. Note that the symmetric windows in Fig. 9 are best suited to minimize $\tilde{\tau}_{12}$.